A level set framework with a shape and motion prior for segmentation and region tracking in echocardiography

Igor Dydenko [a], Fadi Jamal [b], Olivier Bernard [a], Jan D'hooge [c], Isabelle E. Magnin [a], Denis Friboulet [a,*]

[a] *CREATIS, UMR CNRS 5515, INSA, Bâtiment Blaise Pascal, 69621 Villeurbanne Cedex, France*

[b] *Hopital Cardiologique Louis Pradel 59, Blvd. Pinel 69003 Lyon, France*

[c] *Medical Image Computing, Dept. of Electrical Engineering, Catholic University of Leuven, Leuven, Belgium*

Abstract

We describe a level set formulation using both shape and motion prior, for both segmentation and region tracking in high frame rate echocardiographic image sequences. The proposed approach uses the following steps: registration of the prior shape, level set segmentation constrained through the registered shape and region tracking. Registration of the prior shape is expressed as a rigid or an affine transform problem, where the transform minimizing a global region-based criterion is sought. This criterion is based on image statistics and on the available estimated axial motion data. The segmentation step is then formulated through front propagation, constrained with the registered shape prior. The same region based criterion is used both for the registration and the segmentation step. Region tracking is based on the motion field estimated from the interframe level set evolution. The proposed approach is applied to high frame rate echocardiographic sequences acquired in vivo. In this particular application, the prior shape is provided by a medical expert and the rigid transform is used for registration. It is shown that this approach provides consistent results in terms of segmentation and stability through the cardiac cycle. In particular, a comparison indicates that the results provided by our approach are very close to the results obtained with manual tracking performed by an expert cardiologist on a Doppler Tissue Imaging (DTI) study. These preliminary results show the ability of the method to perform region tracking and its potential for dynamic parametric imaging of the heart.

Key words: level set, segmentation, registration, shape prior, tracking, echography, cardiac ultrasound, heart, motion prior

1 Introduction

Recent advances in the field of echographic equipment enable acquisitions at very high frame rates, ranging from 150 to 350 frames per second (fps) (currently, rates of 60 to 80 fps are common in clinical practice). Furthermore, some research interfaces to modern scanners give now access to the radiofrequency (RF) signal, which is the signal available before the envelope detection step used to obtain the conventional grayscale image. In such conditions, it is possible to perform reliable estimation of the local axial tissue velocity, from which mechanical properties of the tissue, such as strain and strain rate, can be derived (D'hooge et al., 2002). Their evolution through the cardiac cycle is a source of valuable information for the assessment of the myocardial viability. One of the limitations of these techniques is the lack of an automatic and robust method for tracking regions of interest (ROI) through the cardiac cycle. This task is currently performed manually by the cardiologist, which makes it laborious and operator-dependent. In this context, the present paper describes a method for automated segmentation of the cardiac muscle and subsequent tracking of ROI in high frame rate echographic sequences. The described technique uses the same kind of data as is available to the cardiologist, that is the envelope (the usually displayed grayscale image) and the axial velocity field.

Segmentation of echocardiographic images is a particularly difficult task, due to the specificities of the ultrasound acquisition: speckle noise, unsharp boundaries related to diffuse scattering and attenuation. These difficulties are amplified in the case of our application: in order to perform high frame rate acquisition, the number of echographic lines is reduced, which implies in turn a reduced sectorial acquisition window to maintain an acceptable lateral resolution. As a consequence, the imaged cardiac structure is only partially present in the sectorial imaging window and moves in and out of that window; a portion of it may moreover be located in the near field of the probe where image quality is very low.

In this context, we propose to perform segmentation and tracking using a level set representation whose evolution is driven by image statistics and constrained by a shape prior. Early versions of this paper appeared in (Dydenko et al., 2003a,b). The main features of our approach are the following:

- The use of a shape prior implies a reliable registration of that shape to the structure to be detected. Due to the above mentioned specificities of echocardiographic images, such a registration cannot be based only on image information. We thus derive a framework where registration is obtained

* Corresponding author (denis.friboulet@creatis.insa-lyon.fr)

through a rigid or an affine transform computed by minimizing a criterion based on image statistics and on the a priori estimated interframe axial velocity.
- Statistical region-based level set evolution is then performed using the registered shape both as initial contour and shape constraint.
- The evolution of the level set is used to estimate the interframe 2D motion field. This motion field is then used to track a particular region of interest in the cardiac muscle.

The present paper is organized as follows. Section 2 describes the related work in the area of echocardiographic image segmentation and discusses the application of the level set framework for this task. Section 3 describes our method of segmentation and tracking. Section 4 details the specific settings made for the application of the method to high frame rate echocardiographic image sequences of the interventricular septum. Section 5 presents results obtained in in vivo sequences and provides preliminary comparative results with a DTI study. Finally, we draw conclusions and perspectives of our work in section 6.

2 Related work

2.1 Echographic image segmentation

Segmentation of echocardiographic images has been a field of very active research over the last decade, and it still remains an open and challenging problem. The envelope image is the one commonly displayed in ultrasound scanners, and many recent works processed directly this kind of image in cardiac applications: Malassiotis and Strinzis (1999) performed detection with an active contour model, Mulet-Parada and Noble (2000) detected discontinuities with a phase-based feature detection method and Papademetris et al. (2001) estimated the deformation of the left ventricle of the heart on 3D ultrasound images. Other researchers extracted textural features, such as the average, variance, contrast, entropy and homogeneity, from the envelope image. Segmentation was then performed, for example, by classifying pixels as either blood or myocardium with a neural network (Binder et al., 1999), or with a snake model (Chen et al., 2000). There have been very few applications of the level set technique dedicated to echographic imaging (contrarily to MR or CT imaging), due to the particularly difficult aspect of these images. Among the existing work, Baillard and Barillot (2000) described a 3D level set model for the segmentation of the carotid in 3D ultrasound images and Lin et al. (2002) developed a method dedicated to segmentation of 3D echocardiographic images, based on separate processing of each 2D slice within a multi-scale approach.

Statistical region-based segmentation (Zhu and Yuille, 1996), segmentation using the level set framework (Osher and Sethian, 1988) as well as region-based segmentation within the level set framework are nowadays techniques well established in the image processing community (Paragios and Deriche, 1999b; Chan and Vese, 2001; Jehan-Besson et al., 2002). These techniques have also been adapted for applications in the field of medical image processing.

Following the aforecited authors, we choose to express our segmentation problem using the level set framework. Furthermore, we adopt in the present work a front-driving term based on the statistics of the image regions, which we assume to follow a Rayleigh distribution, as detailed in section 4.1.

However, due to the inherent lack of any geometrical and topological constraints in the basic level set model, region-based level sets still perform badly in difficult images, where data is incomplete and corrupted with massive noise. Such is often the case in medical imaging, particulary echocardiography.

In order to solve this issue, recent work proposed to introduce shape prior to the evolution of the level sets (Leventon et al., 2000; Tsai et al., 2001; Chen et al., 2001; Rousson and Paragios, 2002; Bresson et al., 2003). This idea is somehow contrary to the philosophy of level sets, and therefore the shape prior cannot be introduced directly into the model, as is done in the case of parametrized active contours. The common approach of these studies consists in constructing a level set representation of the available prior information, and in deriving an additional attraction term from this representation.

The prior shape models are extracted from training sets using principal component analysis, by modeling the mean shape (Chen et al., 2001) and shape variability (Leventon et al., 2000; Tsai et al., 2001; Chen et al., 2001; Bresson et al., 2003). In (Rousson and Paragios, 2002) a variational framework is used to build a Gaussian model, expressing the probability of observing at a pixel location a given value of the embedding function.

In our case, however, the identification of the structure of interest requires additional medical knowledge. For this reason, the prior shape is drawn manually by the cardiologist as a simple initial contour on the initial frame of the sequence, rather than extracted automatically from the available data. It is also noted that, due to the imaging conditions, we are dealing with the segmentation of a small part of the cardiac muscle, which is geometrically fairly simple and exhibits low variability.

During the process of segmentation, the prior must be registered with respect either to the evolving level set or to the processed image. This registration

is generally obtained through a rigid or affine transform, minimizing a distance criterion between the prior shape representation and the object being segmented. In (Leventon et al., 2000) a rigid registration was performed by predicting the position of the prior shape based on the current position of the level set and the image gradient. In (Tsai et al., 2001) this result was obtained by optimizing a criterion which aims at recovering a transform that best maps the evolving interface to the shape prior term. Using a variational approach, a unique energy functional was proposed by (Chen et al., 2001) to formalize both registration of the prior shape (rigid transform and scale) and constrained segmentation. (Bresson et al., 2003) extended the work of (Chen et al., 2001) by integrating the statistical shape model of (Leventon et al., 2000). In (Rousson and Paragios, 2002), the problem of registering the prior shape with the evolving interface was solved by seeking a transform (rigid transform and scale) which minimizes a distance criterion between the prior and the evolving embedding function.

The above cited image-based approaches are efficient for the segmentation of well-defined, complete structures. As mentioned in the introduction, we deal with specific images which contain incomplete information, since the cardiac muscle is only partially present in the imaging window, moves in and out of this window and is corrupted by the near field of the probe. Consequently we introduce the estimated interframe axial velocity as an additional prior in the process of registering the model. This aspect is illustrated in fig. 3 in the experimental section, where we show that the registration process based only on the image information misses the vertical motion of the septum along the sequence.

(Paragios and Deriche, 1999a) proposed to use motion prior to constrain level set-based segmentation. These authors integrate motion estimation and tracking in the front propagation scheme using the assumption of intensity conservation (i.e., the optical Flow constraint). Their approach is based on a motion detection term estimated from the interframe image difference and on a visual consistency term. This last term drives the level set under the constraint of an affine motion, estimated under the assumption of image intensity conservation and using the sum of squared difference.

However, this assumption of image intensity conservation cannot be reliably applied to echocardiographic image sequences, since the changes in the speckle pattern in the envelope echographic image do not reflect the underlying tissue motion (Meunier and Bertrand, 1995). Specific algorithms have been developed for the estimation of tissue velocity either at acquisition time (Doppler Tissue Imaging or DTI), or from the acquired RF sequence (Alam et al., 1998; D'hooge et al., 2000). Due to the conditions of the echographic acquisition (high resolution in the axial direction, low resolution in the lateral direction), these algorithms provide only the axial velocity. Consistently with our applica-

tion, we use the velocity estimated through such approaches as an additional prior in the process of registering the model.

To conclude this section, let us cite the contribution of (Jehan-Besson et al., 2000), who described a method for the estimation of the motion field from a video sequence segmented with level sets. The motion estimation algorithm described in the last part of the methodological section of the present article, useful in the tracking step, is inspired by the work of these investigators.

3 Methodology

We first describe in this section the data term based on image statistics used for image registration and level set-based segmentation. We then detail the three steps involved in the proposed method, that is:

- Registration of the shape prior using image statistics and a priori motion information;
- Level set evolution using the registered shape prior;
- Estimation of the interframe 2D motion field from the evolution of the level sets.

3.1 Region statistics-based curve evolution

Both the registration of the prior shape and the level set evolution are based on image statistics. In this context, we follow the framework initially described by (Zhu and Yuille, 1996) and used by other authors in different applications for statistical region-based segmentation (Paragios and Deriche, 1999b; Paragios et al., 2002). This approach relies on evolving a curve in such a way that the resulting partition of the image maximizes a posterior probability of distribution of the image grey levels in the inside and outside of the detected object.

Let $P_{in}(I(p))$, $P_{out}(I(p))$ be the probability density functions (PDF) of observing the value $I(p)$ at pixel p, in the inside and outside of the object, respectively, and let Γ be the closed curve defined as:

$$[\Gamma : [0, \Lambda] \mapsto \Re^2, s \mapsto p = \Gamma(s)] \tag{1}$$

The problem of finding a partition of the image which maximizes the posterior probability is equivalent to finding the curve Γ which minimizes the following

cost functional:

$$E(\Gamma) = \iint_{\Omega_{in}} -\log P_{in}(I)d\omega + \iint_{\Omega_{out}} -\log P_{out}(I)d\omega \tag{2}$$

where the curve Γ partitions the image domain in two regions: the inside Ω_{in} and the outside Ω_{out}. Using a gradient descent scheme, the minimization of $E(\Gamma)$ is obtained through the evolution of Γ defined by (Zhu and Yuille, 1996):

$$\frac{d\Gamma}{dt} = -\log \frac{P_{in}(I)}{P_{out}(I)} N \tag{3}$$

where N is the vector normal to the curve Γ. We define for further developments the term δ:

$$\delta = -\log \frac{P_{in}(I)}{P_{out}(I)} N \tag{4}$$

The data term δ may be interpreted as a statistical force driving the curve Γ to the desired image partition and thus provides the evolution of Γ at each iteration of the gradient descent scheme. As detailed in section 4.1, we use a Rayleigh PDF to model image statistics of the echocardiographic images.

3.2 Registration of the prior shape

3.2.1 Registration based on image statistics

A powerful way to guide the evolution of an initial shape towards the object to be segmented is to constrain its motion. In this section, we assume that an initial curve Γ has been approximately positioned in the vicinity of the object and this curve is used as a shape prior.

In section 2, we indicated that related work proposed to extract the initial shape from training data sets using principal component analysis. In contrast to these approaches, in our application the initial contour is drawn manually by the cardiologist on the first frame of the sequence. Our choice is primarily motivated by the lack of complete information when choosing the initial contour: indeed, only a part of the muscle visible on the image is interesting from a medical point of view, and that part must be selected by the cardiologist. Also, given the low variability of the muscle shape within one sequence, the contour is geometrically fairly simple.

We address the problem of positioning the shape Γ on the image using a rigid or an affine transform, in the sense of minimizing the posterior segmentation probability (equation 2).

In 2D, the transform parameters thus correspond to a 2×2 matrix M and a 2-component translation vector T. The matrix M corresponds to rotation,

shear and scale in the case of affine registration, whereas it corresponds only to rotation if rigid registration is considered. The transform of any point p is then defined as follows (all vectors are column vectors):

$$p' = Mp + T \tag{5}$$

Let us call $v(p) = (v_x, v_y)$ the motion field induced by the transform at each point p of the interface

$$v(p) = \frac{\partial \Gamma}{\partial t} \tag{6}$$

If one considers the motion of the interface in each iteration as stationary (i.e. the motion field of the interface does not depend on time t), and also supposing without loss of generality that the time step in each iteration is 1, the motion field expresses as follows:

$$v(p) = (M - I_d)p + T \tag{7}$$

where I_d is the identity matrix.

Referring back to the framework described in the previous section, we note that the conventional, unconstrained evolution of Γ is given by the data term δ. We then propose to perform registration in the image in the following way: for each iteration of the gradient descent scheme, we compute the transform $(\hat{M}, \hat{T})$ that best approximate (in the least square sense) the unconstrained evolution as given by δ. Using the parametric representation of Γ, (equation 1), such a transform is thus the solution minimizing:

$$E_{M,T} = \int_\Gamma \left| v(p) - \delta(p) \right|^2 ds \tag{8}$$

By replacing $v(p)$ with expression (7), one obtains:

$$E_{M,T} = \int_\Gamma \left| (M - I_d)p + T - \delta(p) \right|^2 ds \tag{9}$$

This cost function provides a way to perform registration based on image statistics through the data term δ. However, due to the specificities of high frame rate echocardiographic images, registration of the prior shape relying only on image information may fail (see for instance fig. 3 in section 5.2). We therefore propose to further constrain the registration process by introducing a motion prior, as described in the next section.

3.2.2 Registration based on image statistics and displacement field

As mentioned in section 2, the assumption of image intensity conservation cannot be reliably applied to motion analysis in ultrasonic image sequences. In

contrast, ultrasound RF acquisition enables 1D motion field estimation in the axial direction (i.e. parallel to the ultrasound pulse propagation; the geometry of an ultrasound acquisition prohibits easy estimation of velocity in the lateral direction). We therefore propose to constrain the registration process through this 1D motion field estimated a priori. For generality, we give in the following the 2D formulation of the proposed motion prior constraint.

Let us call I^τ the current image in which Γ has to be registered, and $I^{\tau-1}$ the previous image in the sequence. We assume that registration has been performed in image $I^{\tau-1}$. The curve registered in $I^{\tau-1}$ is used as the initial positioning of Γ in I^τ.

Let us call $\eta(p) = (\eta_x(p), \eta_y(p))$ the available a priori motion field, defined over the entire image domain Ω and corresponding to interframe motion estimated between $I^{\tau-1}$ and I^τ. We propose to use the field $\eta(p)$ as a guide to move Γ from its initial position (as provided by registration in frame $I^{\tau-1}$) to the final registered position. This can be done by constraining the transform applied to Γ to yield a motion field close to η. This constraint is introduced by modifying the previous cost function $E_{M,T}$ (eq. 8) through a supplementary term, yielding:

$$E_{M,T} = \alpha \int_\Gamma |v - \delta|^2 \, ds + \beta \iint_{\Omega_{in}} |v - \eta|^2 \, d\omega \tag{10}$$

The first integral is estimated over Γ and corresponds to the influence of image data as defined in the previous section, while the second integral is estimated over the region enclosed by the prior Γ and ensures that the estimated transform applied to Γ provides a motion field close to η. The scalars α and β are weights balancing the influence of image data and motion prior terms.

Given the above-addressed specificity of the ultrasound data (see also section 4), we allow anisotropic weighting of the two terms according to the x and y directions. This anisotropic weighting is easily obtained through the following expression:

$$E_{M,T} = \int_\Gamma (v - \delta)^t \, A \, (v - \delta) \, ds + \iint_{\Omega_{in}} (v - \eta)^t \, B \, (v - \eta) \, d\omega \tag{11}$$

where the 2x2 matrices containing the weights of the two terms in x and y are defined as :

$$A = \begin{pmatrix} \alpha_x & 0 \\ 0 & \alpha_y \end{pmatrix} \qquad B = \begin{pmatrix} \beta_x & 0 \\ 0 & \beta_y \end{pmatrix} \tag{12}$$

The minimum of the cost function $E_{M,T}$ corresponds to the zeros of its derivatives with respect to the parameters of the transform. The obtained expres-

sions are given in the appendix in the case of an affine and a rigid transformation. These expressions are relatively simple and convenient for numerical implementation, since they involve only integrals over Γ and Ω_{in}, which can be easily approximated numerically through summations.

3.3 Evolution of the level set constrained by the a priori shape

Once registration has been performed, we give in the present step more freedom to the evolution of the curve Γ, so as to make the detection of the shape to be segmented more accurate. The evolving curve is driven by the statistical region-based term δ, and constrained to stay close to the registered prior shape Γ^{π}.

We use the now classical formulation of the level sets: the evolving curve Γ is embedded as the zero level set of a higher dimension embedding function,

$$u(p) = \begin{cases} 0 & , p \in \Gamma \\ -D(p,\Gamma) & , p \in \Omega_{in} \\ +D(p,\Gamma) & , p \in \Omega_{out} \end{cases} \tag{13}$$

where $D(p,\Gamma)$ is the Euclidean distance between point p and the curve Γ.

The term describing closeness to the prior shape is expressed as a quadratic attraction function

$$\chi^{^{\pi}}(p \in \Gamma) = \begin{cases} 0 & , p \in \Gamma^{\pi} \\ -|D(p,\Gamma^{\pi})|^2 & , p \in \Omega^{\pi}_{in} \\ +|D(p,\Gamma^{\pi})|^2 & , p \in \Omega^{\pi}_{out} \end{cases} \tag{14}$$

When processing temporal sequences of images, segmentation is carried out simultaneously with one level set evolving on each image. Let $\{u^{\tau}\}, \tau = 1...\Theta$ be the sequence of Θ embedding functions, each one segmenting image I^{τ} from the processed sequence. In order to introduce temporal continuity of the segmented object, we define a term constraining the level sets in consecutive frames. We use the same formulation of the attraction term based on the distance function as the one introduced for the shape prior. Specifically, attraction to the level set previous in the temporal sequence writes as follows:

$$\chi^{\tau,\tau-1}(p \in \Gamma^{\tau}) = \begin{cases} 0 & , u^{\tau-1}(p) = 0 \\ -\left(u^{\tau-1}(p)\right)^2 & , u^{\tau-1}(p) < 0 \\ +\left(u^{\tau-1}(p)\right)^2 & , u^{\tau-1}(p) > 0 \end{cases} \tag{15}$$

A similar term $\chi^{\tau,\tau+1}$ defines the attraction to the next level set in the temporal sequence.

The three previously described terms, χ^{π}, $\chi^{\tau,\tau-1}$ and $\chi^{\tau,\tau+1}$, have been defined only on the curve Γ (i.e. on the zero level set of u). In order to be incorporated into the equation of the level set evolution, they have to be expressed on the entire domain Ω. This is done in the following way:

$$\chi'(p) = \begin{cases} \chi(p) & \text{, if } p \in \Gamma \\ \chi(p_0) | \Big(p_0 \in \Gamma \text{ and } \widehat{pp_0} = D(p,\Gamma) \Big) & \text{, if } p \notin \Gamma \end{cases} \tag{16}$$

where $\widehat{pp_0}$ denotes the distance between p and p_0.

Injecting the previously developed terms in the level set evolution formulation, we obtain the general evolution equation, which incorporates the classical curvature term (κ), the statistical image-based term, a shape prior term and the two temporal consistency terms:

$$\frac{\partial u}{\partial t} = \Big(\lambda_\kappa \kappa + \lambda_\delta \delta + \lambda_\pi \chi'^{\pi} + \lambda_\tau (\chi'^{\tau-1} + \chi'^{\tau+1}) \Big) |\nabla u| \tag{17}$$

3.4 Motion estimation and tracking

We use the result of segmentation to derive the interframe motion field $v^{\tau,\tau+1}(p)$. This motion field is then used to perform the tracking of a region of interest in the segmented structure. For each frame, the motion field is a composition of the motion field corresponding to the registration step, and of the deformation field, corresponding to the evolution of the level set.

Considering a point p of the image domain Ω, let us call q the point obtained by applying the transform to p. The motion field $v_{AF}(p)$ corresponding to this transform is then defined as:

$$q = p + v_{AF}(p) \tag{18}$$

This motion field is easily obtained from equation (7) as:

$$v_{AF}(p) = \Big(\hat{M} - I_d \Big) p + \hat{T} \tag{19}$$

The derivation of the motion field corresponding to the level set evolution is based on the assumption that any point of the embedding function stays on the same level set during its evolution. This approach was proposed by (Jehan-Besson et al., 2000) and interestingly, it is equivalent to applying the optical flow constraint (Horn and Schunck, 1981) to the embedding function.

For a point q, let us call r the corresponding point after the level set evolution. The field $v_{LS}(q)$ describing the motion of point q with the evolving level set is then defined as:

$$r = q + v_{LS}(q) \tag{20}$$

From the above assumption, it is then possible to show that $v_{LS}(q)$ is given by (Jehan-Besson et al., 2000) :

$$v_{LS}(q) = [u_R(q) - u_S(q)] \frac{\nabla u_S(q)}{|\nabla u_S(q)|^2} \tag{21}$$

where u_R and u_S are, respectively, the initial embedding function and the one after convergence of the level set; the motion field v_{LS} is expressed at each point of the domain Ω, since the level set is defined through a continuous function u.

From equations (18) and (20), the total motion field $v(p)$ is given as :

$$v(p) = v_{AF}(p) + v_{LS}(q) = v_{AF} + v_{LS}(p + v_{AF}(p)) \tag{22}$$

Denoting $v^\tau(p)$ and $v^{\tau+1}(p)$ the motion fields associated, respectively, with frame τ and frame $\tau+1$, the interframe motion field $v^{\tau,\tau+1}(p)$ is then computed as:

$$v^{\tau,\tau+1}(p) = v^{\tau+1}(p) - v^\tau(p) \tag{23}$$

4 Application to high frame rate septal echocardiographic data

The previously described framework is applied to high frame rate echocardiographic image sequences of the interventricular septum. In each case the echographic device was equipped with an RF interface, so the data were initially available as a sequence of RF signals. We describe in this section the specific settings made for this application.

The a priori 1D motion field used to constrain the registration scheme is estimated from the RF signals using a technique known from the literature (Alam et al., 1998; D'hooge et al., 2000). This technique consists in tracking RF patterns in consecutive temporal RF lines along the pulse propagation direction (axial direction). The tracking is made adaptive by applying temporal pre-stretching to the reference RF pattern in order to take into account the deformation of the RF signal due to the motion of the myocardium.

From the RF signals, the envelope echocardiographic images are computed, without logarithmic compression in order to preserve statistical properties (see section 4.1 below).

As discussed in section 3.2.1, the prior shape is drawn manually by the cardiologist as an initial contour on the initial frame of the sequence.

Registration of the prior shape in each image of the sequence is then performed using a rigid transform: indeed, the deformation of the septal muscle during the cardiac cycle is relatively small as compared to its overall motion (translation and rotation). This can be visually evaluated from the video corresponding to fig. 4, available in the online version of the paper at doi: XXXXXXXX and at www.creatis.insa-lyon.fr/ ˜ frib/media_04. Once registration is performed, the deformation of the myocardium is captured in the second step of the segmentation process, that is during free motion of the level-set. As shown in the result section, this yields consistent segmentation and tracking.

The approach implies the selection of the PDF modelling the statistics of the echocardiographic images through the data term δ (eq. 4), as well as the choice of the hyperparameters involved in the registration step (eq. 11) and in the expression governing the evolution of the level set (eq. 17). These aspects are described in the following subsections.

4.1 Statistical distribution

In the context of our work it is crucial to carefully model the intensity distribution of ultrasound envelope images through an adequate PDF. It has been shown (Wagner et al., 1983) that for a large enough density of scatters, the image speckle is fully developed and the distribution of intensities follows the Rayleigh PDF:

$$P(I) = \frac{I}{\sigma^2} e^{\frac{-I^2}{2\sigma^2}} \tag{24}$$

Such a choice is common in the field of region-based segmentation of echographic images (Guerault et al., 2000; Haas et al., 2000).

The registration and segmentation method requires initial estimation of the statistical parameters (σ_{in}, σ_{out}) of the Rayleigh distributions in the two region of the envelope image, and it is not a trivial task. The determined prior shape does not partition the image into two statistically meaningful regions, namely muscle and blood. Indeed, uninteresting muscular structures, whose gray level distributions are similar to the one of the muscle of interest, are present in the image and remain outside of the prior shape.

The best partition of the sequence in two statistically distinct regions could be obtained by segmenting independently each frame with a region-based Rayleigh term. However, this would be a computationally expensive task, considering that the estimation of statistical parameters is only a preliminary stage of processing.

We introduce a different approach, where the sequence of images is considered as a single multichannel image, representing several acquisitions of the same object. Indeed, the heart muscle has a cyclic motion, whose amplitude does not exceed by far the size of the muscle itself. Consequently, it stays within a constrained region of the image. Inspired by the work of Germain and Refregier (1999), we propose to process the multichannel image by segmenting a unique image, which is the average of all the channels.

We propose to use the result of segmentation of the average envelope image as an approximation of the best partition, and the statistical distribution parameters are estimated as follows:

- the image corresponding to the envelope of the average of the RF image sequence is computed. Under the assumption of fully developed speckle, the RF signals follow a Gaussian distribution and the average of these signals is also Gaussian-distributed. Taking the envelope of the average results then in a Rayleigh-distributed image,
- segmentation of this image with a Rayleigh region-based term, where the statistical parameters of the distributions are not known a priori and are re-estimated at each iteration,
- use of this segmentation to partition the sequence considered here as a volume and calculation of a unique set of parameters from all the pixels of the sequence belonging to the inside and outside, respectively.

The set of parameters obtained in this way is used both during the registration and the segmentation step, in all the frames.

4.2 Settings of the hyperparameters

The registration step implies the choice of the relative weights of the image data and motion prior terms in equation (11). The specificities of our data (a priori 1D velocity field avaible only along the axial direction) make this choice relatively easy: registration along the axial direction (y axis in the images) is performed using the velocity field-based term, and the image-based term guides registration in the lateral direction (x axis in the images), so we set $(\alpha_x, \alpha_y) = (1, 0)$ and $(\beta_x, \beta_y) = (0, 1)$.

The segmentation step requires tuning several weighting hyperparameters, which set the influence of each term of the level set evolution. We observed that the choice of an optimal set of parameters is relatively easy, and the method is not very sensitive to small deviations from the adopted values. In practice, when segmenting experimental echocardiographic acquisitions (180 - 600 frames), we performed tests on short series of frames extracted from the sequence. The determined values of parameters could then be used throughout

the sequence, without the need of further tuning.

5 Results on in vivo echocardiographic data

5.1 In vivo data sets

In this section, we present results obtained in two echocardiographic sequences sequences (Sequence A and Sequence B) acquired in the apical four-chamber view. Such acquisitions are used in clinical practice to assess functional characteristics of the septal wall, which is positioned in the central part of the image. The data sets were acquired for the purpose of obtaining high frame rate sequences, enabling reliable estimation of the axial velocity. As pointed out in the introduction, their visual quality is consequently not optimal. Segmentation and tracking results obtained from sequence A are qualitatively, visually assessed by a medical expert. Sequence B is used to study the time evolution of a specific parameter (the local velocity) and provides a more quantitative evaluation by comparing our approach with the manual tracking performed by an expert cardiologist on a DTI study.

Fig. 1 presents example frames extracted from the two sequences with indicated cardiac structures, along with the estimated axial velocity field.

In these images (see also fig. 4), it is to be noted that the connection of the septum with the anterior and posterior wall is almost lost, and that the septum thus appears as an isolated, elongated structure. As mentioned earlier, this is linked to the acquisition configuration: due to high frame rate acquisition, the imaging window angle is reduced and the imaged area is still smaller near the probe, where the connexion of the septum with the anterior and posterior wall is located in apical acquisitions. This region is moreover located in the near field of the probe where image quality is very low. It is to be noted that the segmentation and tracking results given in fig. 4, 6 and 9 in the next sections may also be evaluated visually from the videos available in the online version of the paper at doi: XXXXXXXX and at
http://www.creatis.insa-lyon.fr/ ˜ frib/media_04.

5.2 Sequence A

The sequence was acquired from a young healthy volunteer, with a Toshiba PowerVision 6000 (Toshiba Medical Systems, Otawara, Japan), equipped with an RF interface for research purposes, which allows continuous acquisition of

digital IQ data. Each frame is composed of 60 adjacent RF lines, with an acquisition sector of approximately 45 degrees. The frame rate was 150 images per second and a sequence of 187 RF images was obtained. A 3.75 MHz-probe was used in this study, insonifying with a pulse of central frequency $f_0 = 2.5$ MHz.

As previously described, the statistical parameters used for registration and segmentation were obtained from a pre-segmentation of the average image of the sequence. The initial contour was manually drawn in one frame from the sequence. Processing was performed as described in the methodological section. Segmentation steps (registration and free evolution of the level set) are shown in one frame in fig. 2, and one can observe how each step improves the result.

Fig. 3 illustrates the influence of the velocity term in three frames, extracted from the sequence, by showing the result of registration with and without the velocity term (for better viewing, an arrow indicates the position of the mitral valve - septum connexion in each frame). When velocity information is used (fig. 3, left), the contour correctly follows the axial motion of the muscle (along the vertical axis in the images). When velocity information is not used (fig. 3, right), registration yields a drift in the axial direction and finally fails to properly follow the cardiac structures (compare the relative position of the contour and the arrow in fig. 3, frame 71 left and frame 71 right).

Fig. 4 shows eight frames extracted from the sequence along with the obtained results of segmentation. In all the frames, the contour matches the muscle very well. It is particularly encouraging that segmentation is correct in the upper part of all the images, where contrast is extremely poor due to the ultrasonic near field: this is made possible only because of the prior shape. In several frames, additional cardiac structures (the valves) move close to the septum. However, again owing to the shape prior, the interface stays bounded to the septum. The sequence starts with the isovolumetric contraction phase (frame 4), and one can appreciate how the contour moves and rotates along with the contracting and shortening muscle in the ejection phase (frames 38 and 66). The muscle is relatively still in diastasis (frames 109 and 128): the detected contour is stable, and tiny phenomena such as the muscle's flexion are accurately captured. Finally, frame 149 corresponds in the next cardiac cycle to the same instant as frame 4. The detected contours in the two frames are very similar.

The result of segmentation is then used to obtain the motion field of the object (fig. 5). Frame ($4 \rightarrow 14$) corresponds to the beginning of isovolumetric contraction, and therefore there is little motion of the muscle. In the ejection phase ($38 \rightarrow 48$; $66 \rightarrow 76$), the fast contraction of the septum and its motion towards reducing the volume of the left ventricle (positioned in the

right-hand side of the image) can be clearly appreciated. During the end of isovolumetric relaxation and beginning of early filling (79 → 89), the return of the muscle to its previous position is visible, and in early filling, the septum increases the volume of the left ventricle by moving outwards (91 → 101). The two next frames (109 → 119 and 128 → 138) correspond to a still phase of diastasis, and little motion can be seen. The obtained motion field seems therefore qualitatively consistent with the different phases of the cardiac cycle and the expected motion of the septum. It was subsequently used to track a manually placed circular ROI (see fig. 6). The position of the region follows the translation and deformation of the septum. It can be remarked that the size of the ROI varies little throughout the cycle, which is an indicator of stability and homogeneity of the motion field. It is very interesting to note that the ROI does not drift towards the cardiac cavities, despite the fact that the septum in the images is very thin. The results obtained on this data set have been positively evaluated by an expert cardiologist through qualitative, visual inspection.

5.3 Sequence B : preliminary comparative results

The ultimate goal of the method described here is to obtain the evolution of mechanical tissue parameters, such as the axial velocity, strain or strain rate (D'hooge et al., 2000), in particular regions of the cardiac muscle. The evolution of these parameters is used for the assessment of myocardial function, and it is obtained by the physician from specific acquisitions and with a dedicated software. The scheme in fig. 7 summarizes this procedure. The analysis is based on a DTI acquisition of a velocity cardiac sequence. In a subsequent off line processing of the data set with a dedicated software, the cardiologist performs manual tracking of control points through the cardiac cycle. The software then generates curves of evolution of the parameters of interest in these control points. Tracking is necessary in order to follow the same part of the muscle through the cycle, and this task, performed manually in sequences of 200 to 400 frames, is extremely tedious.

DTI is thus used in this section as a reference for velocity estimation. Using a rotating phantom experiment (Kukulski et al., 2000) indeed showed a very good agreement between DTI and true velocities (correlation coefficient of 0.99), although DTI tends to underestimate the velocity values (1.35 0.36 cm/s for velocities ranging from 1.6 to 38 cm/s). As a consequence the absolute values delivered through DTI should be used with care (due to the underestimation), but relative values may be used with a good confidence.

In an attempt to evaluate the ability of the method to produce medically meaningful results, the temporal evolution of one tissue parameter was ob-

tained in a ROI with the use of our method, and compared to the evolution of the same parameter in the same ROI obtained by an expert cardiologist with a setup described above. The chosen tissue parameter is the axial velocity, which is used for the assessment of the myocardial contractile function.

Processed data were acquired with a GE Vingmed, System V (Horten, Norway) equipped with a RF output, used in clinical routine, and a cardiac probe of central frequency 2.22 MHz was used. A DTI acquisition was performed, which is a built-in feature of the Vingmed scanner. A RF acquisition was performed shortly afterwards, in the same patient and in the same view, at 98 fps, with each frame containing 26 RF lines over an angle of 31 degrees. It is to be noted that, due to the use of another acquisition setup, the frame rate and the number of RF lines are low as compared to previously processed data.

Fig. 8 presents a screen-shot from the dedicated software used by the cardiologist, and three control points are visible upon the septum. From the DTI acquisition, the axial velocity field in control point 2 was obtained by the cardiologist.

In parallel, the segmentation procedure discussed in previous sections was applied to the RF data set. A ROI was then defined in such a way that it corresponds to the central control point (number 2) from fig. 8. Tracking was finally performed, and the resulting positions of the ROI are presented in fig. 9. Subsequently, the evolution of the axial velocity field in the tracked region was computed, by averaging in each frame the velocity values under the ROI.

Fig. 10 presents the curve obtained automatically with our method, superimposed on the curve provided by the expert cardiologist. There is a very good concordance of the two results; the overall aspect of the two plots is similar and extreme values of velocities are almost identical. Characteristic short cardiac events, such as isovolumetric contraction, isovolumetric relaxation or the peak velocity in ejection coincide in the two plots. Let us also note a good stability of the result obtained with our method over two consecutive cycles.

One limitation of the described procedure is that the frame rate of the available RF data is relatively low (98 fps), as compared to the dedicated DTI acquisition (200 fps). As a consequence, some short events of the cardiac cycle may be missed. For example, the extreme negative velocity in late filling is not the same in the two curves, and it seems that the negative peak has been overlooked in the RF acquisition because of the low temporal resolution.

6 Conclusion and perspectives

We have described in this paper a method for segmentation and tracking in high frame rate echocardiographic images. The difficulty of this task is linked to the specificity of these acquisitions, where the cardiac structure of interest is only partially visible, move in and out of the imaging field and is moreover corrupted by the near field of the probe. In this context, we have proposed to perform segmentation using a level set representation whose evolution is guided by image statistics and constrained by shape a priori. This strategy implies a reliable registration of the a priori to the structure to be detected. Such a registration is obtained through a rigid or affine transform which is computed by minimizing a global region-based criterion based on image statistics and on the estimated interframe motion. The tracking of a region of interest is then obtained by using the motion field estimated from the level set evolution.

The method has been applied to the segmentation of the septum. In the present implementation, an initial contour is determined on the first image of the sequence and is used as the shape prior. The determination of this contour is the only interaction required from the operator, subsequent registration and segmentation steps being fully automatic.

The approach has been tested on two sequences acquired in vivo and have led to very encouraging experimental results. Results obtained on the first sequence indicate that the segmentation and the tracking are visually consistent and reliable with respect to the cardiac motion. In particular, the tracking of a ROI was found to be stable insofar as it does not yield any drift of the ROI outward the thin structure of the septum. The second sequence was used to study the time evolution of a specific parameter, the local velocity, by tracking a ROI in the septum. This sequence represented a difficult case, because of lower image quality and lower frame rate. The results provided by our approach were found to be very close to the results obtained with manual tracking performed by an expert cardiologist from a DTI study. Moreover, these results appeared to be stable and reproducible with respect to the cardiac cycle period. These promising results should however be considered as preliminary: future work includes the implementation of the method in a clinical research environment in order to validate its reliability on the basis of a larger number of data sets. The approach is currently implemented without any particular optimisation for registration. The segmentation step (i.e. evolution of the level-set) is done using the sparse field technique (Whitakker , 1998). Using a Pentium 4 processor running at 3.00 Ghz, this yields a typical computation time of about 50 mn for 100 frames. Though this implies offline processing, it has to be kept in mind that it still advantageously replaces the tedious task of manual tracking through the whole sequence.

The medical interest of the proposed method is to provide the access to the evolution of local myocardial mechanical properties, such as velocity or strain. In that sense, the developed method answers a direct medical need. From the obtained preliminary results, it appears that the method could thus, in perspective, provide an efficient tool for dynamic parametric imaging of the myocardium in echocardiography. A unique RF acquisition could be the basis for image segmentation, region tracking and finally for the derivation of the time evolution of parameters assessing myocardial properties.

Appendix

Affine registration

Let us note

$$M = \begin{pmatrix} a & b \\ c & d \end{pmatrix} \qquad T = \begin{pmatrix} t_x \\ t_y \end{pmatrix} \tag{25}$$

The minimum of $E_{M,T}$ corresponds to the zeroes of its derivative with respect to the six parameters a, b, c, d, t_x and t_y. By developping (eq. 11), these derivatives may be expressed as a function of integrals of p, δ and η over Γ and Ω.

Let us define the following matrices, vectors and scalars;

$$IN^{\Gamma} = \int_{\Gamma} pp^t ds \qquad IN^{\Omega} = \int_{\Omega} pp^t d\omega \tag{26}$$

$$G^{\Gamma} = \int_{\Gamma} p ds \qquad G^{\Omega} = \int_{\Omega} p d\omega \tag{27}$$

$$L = \int_{\Gamma} ds \qquad S = \int_{\Omega} d\omega \tag{28}$$

$$\overline{\delta} = \begin{pmatrix} \overline{\delta}_x \\ \overline{\delta}_y \end{pmatrix} = \int_{\Gamma} \delta ds \qquad \overline{\eta} = \begin{pmatrix} \overline{\eta}_x \\ \overline{\eta}_y \end{pmatrix} = \int_{\Omega} \eta d\omega \tag{29}$$

$$P\Delta_x = \int_{\Gamma} \delta_x p ds \qquad PN_x = \int_{\Omega} \eta_x p d\omega \tag{30}$$

$$P\Delta_y = \int_{\Gamma} \delta_y p ds \qquad PN_y = \int_{\Omega} \eta_y p d\omega \tag{31}$$

where the integral of a matrix (resp. vector) is to be understood as the integral of each term of the matrix (resp. vector)

Let us now gather the six unknowns in the two following vectors

$$V_x = \begin{pmatrix} a \\ b \\ t_x \end{pmatrix} \qquad V_y = \begin{pmatrix} c \\ d \\ t_y \end{pmatrix} \tag{32}$$

Using elementary algebraic computations, it can be then shown that the unknowns parameters are obtained as the solutions of the two following 3×3 linear systems:

$$\begin{cases} A_x V_x + B_x = 0 \\ A_y V_y + B_y = 0 \end{cases} \tag{33}$$

where

$$A_x = \alpha_x \begin{pmatrix} IN^\Gamma & G^\Gamma \\ \left(G^\Gamma\right)^t & L \end{pmatrix} + \beta_x \begin{pmatrix} IN^\Omega & G^\Omega \\ \left(G^\Omega\right)^t & S \end{pmatrix} \tag{34}$$

$$B_x = \alpha_x \begin{pmatrix} P\Delta_x \\ \overline{\delta}_x \end{pmatrix} + \beta_x \begin{pmatrix} PN_x \\ \overline{\eta}_x \end{pmatrix} \tag{35}$$

$$A_y = \alpha_y \begin{pmatrix} IN^\Gamma & G^\Gamma \\ \left(G^\Gamma\right)^t & L \end{pmatrix} + \beta_y \begin{pmatrix} IN^\Omega & G^\Omega \\ \left(G^\Omega\right)^t & S \end{pmatrix} \tag{36}$$

$$B_y = \alpha_y \begin{pmatrix} P\Delta_y \\ \overline{\delta}_y \end{pmatrix} + \beta_y \begin{pmatrix} PN_y \\ \overline{\eta}_y \end{pmatrix} \tag{37}$$

Rigid registration

In the case of a rigid registration, M corresponds to a rotation matrix, i.e.

$$M = \begin{pmatrix} cos\theta & -sin\theta \\ sin\theta & cos\theta \end{pmatrix} \tag{38}$$

where θ is the rotation angle.

The solution thus corresponds to the zeroes of the derivatives of $E_{M,T}$ with respect to θ, t_x, t_y.

Let us note $(x\ y)$ the coordinates of a point p and let us note

$$m_{pp} = \begin{pmatrix} -xy & x^2 \\ xy & y^2 \end{pmatrix} \qquad m_p = \begin{pmatrix} -y & x \\ x & y \end{pmatrix} \tag{39}$$

$$m_{\delta_p} = \begin{pmatrix} -y\delta_x & x\delta_x \\ x\delta_y & y\delta_y \end{pmatrix} \qquad m_{\eta_p} = \begin{pmatrix} -y\eta_x & x\eta_x \\ x\eta_y & y\eta_y \end{pmatrix} \tag{40}$$

Let us then define the following matrices:

$$M_{pp}^{\Gamma} = \int_{\Gamma} m_{pp} ds \qquad M_{pp}^{\Omega} = \int_{\Omega} m_{pp} d\omega \tag{41}$$

$$M_{p}^{\Gamma} = \int_{\Gamma} m_{p} ds \qquad M_{p}^{\Omega} = \int_{\Omega} m_{p} d\omega \tag{42}$$

$$M_{\delta_p}^{\Gamma} = \int_{\Gamma} m_{\delta_p} ds \qquad M_{\eta_p}^{\Omega} = \int_{\Omega} m_{\eta_p} d\omega \tag{43}$$

Let us moreover define the vector

$$V_\theta = \begin{pmatrix} cos\theta \\ -sin\theta \end{pmatrix} \tag{44}$$

The translation T can then be shown to be given as

$$T = DV_\theta + E \tag{45}$$

where

$$D = -K^{-1} \left(\alpha M_p^{\Gamma} + \beta M_p^{\Omega} \right) I_c \tag{46}$$

$$E = -K^{-1} \left(\alpha \left(\overline{\delta} - G^{\Gamma} \right) + \beta \left(\overline{\eta} - G^{\Omega} \right) \right) \tag{47}$$

$$K = \alpha L + \beta S \tag{48}$$

$$I_c = \begin{pmatrix} 0 & -1 \\ 1 & 0 \end{pmatrix} \tag{49}$$

The rotation angle θ can then be shown to fulfill the following equation

$$-V_\theta^t \left(A - D^t C\right) V_\theta + \left(B + E^t C\right) V_\theta = 0 \tag{50}$$

where

$$\begin{aligned} A &= \alpha_x IN^\Gamma + \alpha_y I_c IN^\Gamma + \beta_x IN^\Omega + \beta_y I_c IN^\Omega \\ B &= (\alpha_x \;\; \alpha_y)\left(M_{\delta_p}^\Gamma - M_{pp}^\Gamma\right) + (\beta_x \;\; \beta_y)\left(M_{\eta_p}^\Omega - M_{pp}^\Omega\right) \\ C &= \alpha M_p^\Gamma + \beta M_p^\Omega \end{aligned}$$

From equation (50), the rotation angle θ then corresponds to the roots of a second degree polynomial in $cos\theta$, $sin\theta$.

References

Alam, S. K., Ophir, J., Konofagou, E., 1998. An adaptive strain estimator for elastography. IEEE Transactions on Ultrasonics, Ferroelectricity and Frequency Control 45, 461–472.

Baillard, C., Barillot, C., 2000. Robust 3d segmentation of anatomical structures with level sets. In: Delp, S. L., DiGioia, A. M., Jaramaz, B. (Eds.), Proceedings of Medical Image Computing and Computer-Assisted Intervention - MICCAI, Third International Conference, Pittsburgh, Pennsylvania, USA, October 11-14, 2000. Vol. 1935 of Lecture Notes in Computer Science. Springer, pp. 236–245.

Binder, T., Suessner, M., Moertl, D., Strohmer, T., Baumgartner, H., Maurer, G., Porenta, G., 1999. Artificial neural networks and spatial temporal contour linking for automated endocardial contour detection on echocardiograms: a novel approach to determine left ventricular contractile function. Ultrasound in Medicine and Biology 25 (7), 1069–1076.

Bresson, X., Vandergheynst, P., Thiran, J., 2003. A Priori Information in Image Segmentation: Energy Functional based on Shape Statistical Model and Image Information. Proceedings of International Conference on Image Processing 2003, ICIP'03, Barcelona, Spain, Vol. 3, pp. 428-431, September 2003.

Chan, T. F., Vese, L. A., 2001. Active contours without edges. IEEE Transactions on Image Processing 10 (2), 266–277.

Chen, C.-M., Lu, H. H.-S., Lin, Y.-C., 2000. An early vision-based snake model for ultrasound image segmentation. Ultrasound in Medicine and Biology 26 (2), 273–285.

Chen, Y., Thiruvenkadam, S., Tagare, H. D., Huang, F., Wilson, D., Geiser, E. A., 2001. On the incorporation of shape priors into geometric ac-

tive contours. In: IEEE Workshop on Variational and Level Set Methods (VLSM'01), Vancouver, Canada, July 13, 2001. pp. 145–152.

D'hooge, J., Heimdal, A., Jamal, F., Kukulski, T., Bijnens, B., Rademakers, F., Hatle, L., Suetens, P., Sutherland, G., 2000. Regional strain and strain rate measurements by cardiac ultrasound: principles, implementation and limitations. European Journal of Echocardiography 1 (3), 154–170.

D'hooge, J., Konofagou, E., Jamal, F., Heimdal, A., Barrios, L., Bijnens, B., Thoen, J., de Werf, F. V., Sutherland, G., Suetens, P., 2002. Two-dimensional ultrasonic strain rate measurement of the human heart in vivo. IEEE Transactions on Ultrasonics, Ferroelectrics, and Frequency Control 49 (2), 281–286.

Dydenko, I., Chehbi, S., Friboulet, D., Clarysse, P., D'hooge, J., B.Bijnens, Magnin, I. E., 2002. Using an elastic deformable template for the segmentation of ultrasound cardiac radio frequency images based on the velocity information. In: Proceedings of IEEE International Ultrasonics Symposium, Munich, Germany, October 8-11, 2002. pp. 1706–1709.

Dydenko, I., Friboulet, D., D'hooge, J., Bijnens, B., Magnin, I., 2003a. Segmentation and tracking of the cardiac muscle in echocardiographic sequences using a level set approach. In: Proceedings of IEEE International Ultrasonics Symposium, Hawai, USA, 2003. p. accepted.

Dydenko, I., Friboulet, D., Gorce, J.-M., D'hooge, J., B.Bijnens, Magnin, I. E., 2003b. Towards ultrasound cardiac image segmentation based on the radiofrequency signal. Medical Image Analysis 7 (3), 353–367.

Dydenko, I., Friboulet, D., Magnin, I., 2003c. A variational framework for affine registration and segmentation with shape prior: application in echocardiographic imaging. In: Faugeras, O., Paragios, N. (Eds.), Proceedings of the 2nd IEEE Workshop on Variational, Geometrical and Level Set Methods in Computer Vision, Nice, France, October 11-12, 2003. pp. 201–208.

Germain, O., Refregier, P., 1999. Snake-based method for the segmentation of object in multichannel images degraded by speckle. Optics letters 24 (12), 814–816.

Gronningsaeter, A., Angelsen, B. A. J., Heimdal, A., Torp, H. G., 1996. Vessel wall detection and blood noise reduction in intravascular ultrasound imaging. IEEE Transactions on Ultrasonics, Ferroelectrics and Frequency Control 43 (3), 359–369.

Guerault, G., Delachartre, P., Finet, G., Magnin, I. E., 2000. Modélisation et segmentation d'images échographiques endovasculaires. Traitement du Signal 17 (5-6), 517–529.

Haas, C., Ermert, H., Holt, S., Grewe, P., Machraoui, A., Barmeyer, J., 2000. Segmentation of 3d intravascular ultrasonic images based on a random field model. Ultrasound in Medicine and Biology 26 (2), 297–306.

Horn, B., Schunck, B., 1981. Determining optical flow. Artificial Intelligence 17, 185–203.

Jehan-Besson, S., Barlaud, M., Aubert, G., 2000. Detection and tracking of

moving objects using a new level set based method. In: 15th International Conference on Pattern Recognition, Barcelona, Spain, September 3-8, 2000. IEEE Computer Society.

Jehan-Besson, S., Barlaud, M., Aubert, G., 2002. Dream's: Deformable regions driven by an eulerian accurate minimization method for image and video segmentation. Tech. Rep. 42001-14, I3S.

Kukulski, T., J.U. Voigt, et al. 2000. A comparison of regional myocardial velocity information derived by pulsed and color Doppler techniques: An in vitro and in vivo study. Echocardiography 17(7): 639-651.

Leventon, M., Grimson, E., Faugeras, O., 2000. Statistical shape influence in geodesic active contours. In: IEEE Computer Society Conference on Computer Vision and Pattern Recognition (CVPR), Hilton Head Island, South Carolina, June 13-15, 2000. pp. 1316–1323.

Li, W., v. d. Steen, A. F. W., Lancee, C. T., Honkoop, J., Gussenhoven, E. J., Bom, N., 1996. Temporal correlation of blood scattering signals in vivo from radiofrequency intravascular ultrasound. Ultrasound in Medicine and Biology 22 (5), 583–590.

Lin, N., Yu, W., Duncan, J. S., 2002. Combinative multi-scale level set framework for echocardiographic image segmentation. In: Medical Image Computing and Computer-Assisted Intervention (MICCAI), 5th International Conference, Tokyo, Japan, September 25-28, 2002. pp. 682–689.

Malassiotis, S., Strinzis, M. G., 1999. Tracking the left ventricle in echocardiographic images by learning heart dynamics. IEEE Transactions on Medical Imaging 18 (3), 282–290.

Meunier, J., Bertrand, M., 1995. Ultrasound texture motion analysis: theory and simulation. IEEE Transactions on Medical Imaging 14 (2), 293–300.

Mikic, I., Krucinski, S., Thomas, J. D., 1998. Segmentation and tracking in echocardiographic sequences: active contours guided by optical flow estimates. IEEE Transactions on Medical Imaging 17 (2), 274–284.

Moreau, V., Cohen, L. D., Pellerin, D., 2001. Deformation field estimation for the cardiac wall using doppler tissue imaging. In: Katila, T. (Ed.), First International Workshop on Functional Imaging and Modeling of the Heart FIMH'01, Helsinki, Finland, November 15-16, 2001. Vol. 2230 of Lecture Notes in Computer Science. Springer, pp. 53–60.

Mulet-Parada, M., Noble, J. A., 2000. 2d+t acoustic boundary detection in echocardiography. Medical Image Analysis 4, 21–30.

Osher, S., Sethian, J. A., 1988. Front propagating with curvature dependent speed: algorithms based on hamilton-jacobi formulations. Journal of computational physics 79, 12–49.

Papademetris, X., Sinusas, A. J., Dione, D. P., Duncan, J. S., 2001. Estimation of 3d left ventricular deformation from echocardiography. Medical Image Analysis 5, 17–28.

Paragios, N., Deriche, R., 1999a. Geodesic active regions for motion estimation and tracking. Tech. Rep. 3631, INRIA.

Paragios, N., Deriche, R., 1999b. Geodesic active regions for supervised textu-

ral segmentation. In: IEEE International Conference on Computer Vision, Kerkyra, Corfu, Greece, September 20-25, 1999. pp. 926–938.

Paragios, N., Deriche, R., 2000. Geodesic active contours and level sets for the detection and tracking of moving objects. IEEE Transactions on Pattern Analysis and Machine Intelligence 22, 266–280.

Paragios, N., Rousson, M., Ramesh, V., 2002. Knowledge-based registration and segmentation of the left ventricle: A level set approach. In: IEEE Workshop on Applications in Computer Vision, Orlando, Florida, USA, December 3-4, 2002.

Rabben, S. I., Torp, A. H., Stoylen, A., Slordahl, S., Bjornstad, K., Haugen, B. O., Angelsen, B., 2000. Semiautomatic contour detection in ultrasound m-mode images. Ultrasound in Medicine and Biology 26 (2), 287–296.

Rousson, M., Paragios, N., 2002. Shape priors for level set representations. In: European Conference in Computer Vision, Copenhagen, Denmark, May 27-31, 2002, Proceedings Part II. pp. 78–92.

Sethian, J. A., 2000. Level set methods and fast marching methods. Cambridge University Press.

Suri, J. S., Singh, S., Laximinarayan, S., Zeng, X., Liu, K., Reden, L., 2001. Shape recovery algorithms using level sets in 2-d/3-d medical imagery: A state-of-the-art review. IEEE Transactions on Information Technology in Biomedicine (ITB) 6 (1), 8 –28.

Tsai, A., Yezzi, A., Wells, W., Tempany, C., Tucker, D., Fan, A., Grimson, A., Willsky, A., 2001. Model-based curve evolution technique for image segmentation. In: IEEE Computer Society Conference on Computer Vision and Pattern Recognition (CVPR), Hawaii, December 8-14, 2001. pp. 463–468.

Wagner, R. F., Smith, S. W., Sandrik, J. M., Lopez, H., 1983. Statistics of speckle in ultrasound b-scans. IEEE Transactions on Sonics and Ultrasonics 30 (3), 156–163.

Whitakker, R. T., 1998. A Level-Set Approach to 3D Reconstruction from Range Data. International Journal of Computer Vision, vol.29 (3), pp. 203–231.

Yezzi, A., Zollei, L., Kapur, T., 2003. A variational framework for integrating segmentation and registration through active contours. Medical Image Analysis 7, 171–185.

Zhu, S. C., Yuille, A., 1996. Region competition: Unifying snakes, region growing and bayes/mdl for multi-band image segmentation. IEEE Transactions on Pattern Analysis and Machine Intelligence 18 (9), 884–900.

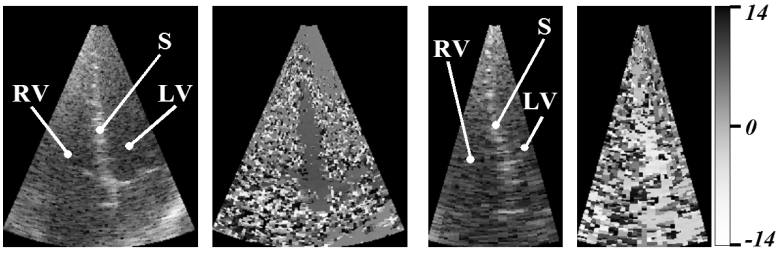

Fig. 1. Example envelope image and velocity field extracted from the sequence acquired at 150 fps (left) and at 98 fps (right). The velocity scale is expressed in cm/s, and common for both acquisitions

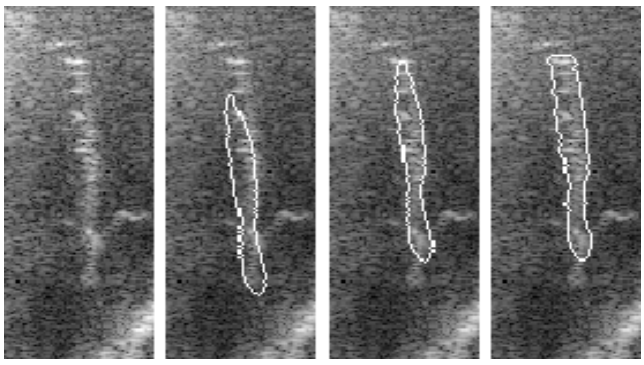

Fig. 2. Steps of the segmentation process in frame 79; from left to right: the envelope image, the initial position of the contour, its position after rigid registration, and the final result of segmentation

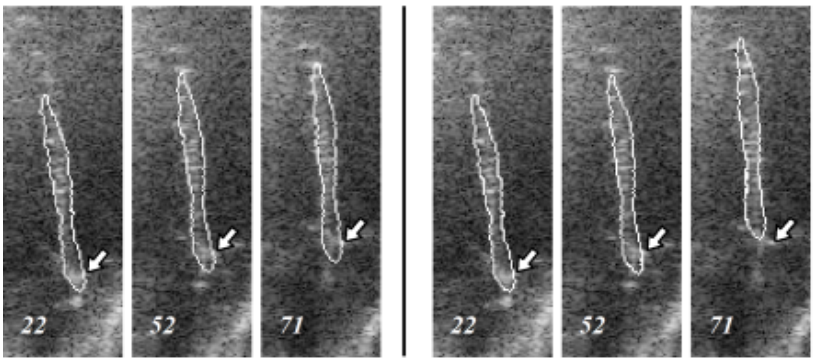

Fig. 3. Illustration of the importance of introducing velocity to registration: results in three frames of translation constrained by the axial velocity field (left) and unconstrained (right). For better viewing, an arrow indicates the location of the mitral valve - septum connexion in each frame. When velocity information is not used (right), registration yields a drift in the axial direction and finally fails to properly follow the cardiac structures (right, frame 71)

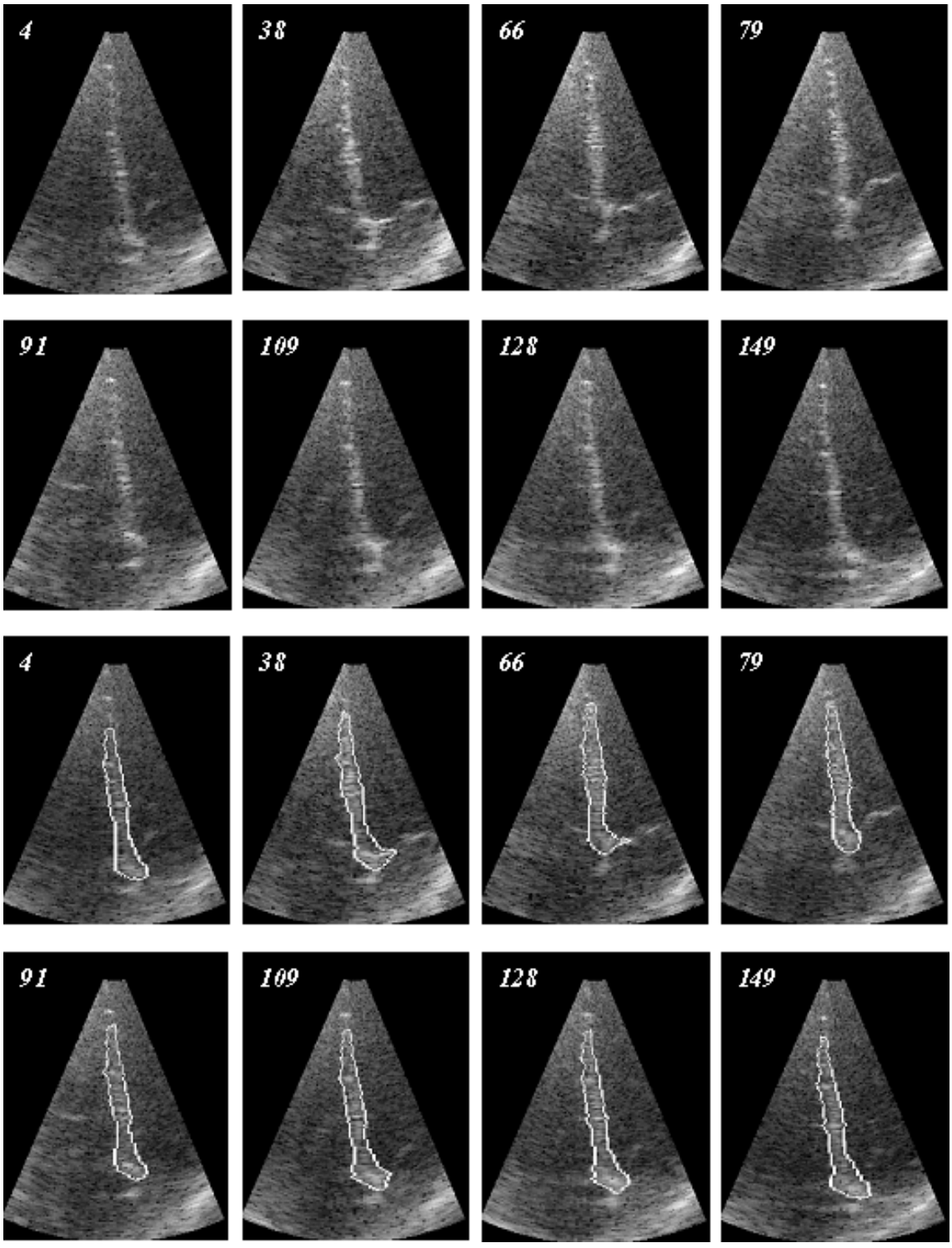

Fig. 4. The result of segmentation in eight frames extracted from the sequence, covering the entire heart cycle; frame 149 corresponds to frame 4 in the next cardiac cycle (numbers indicate frame position in the sequence)

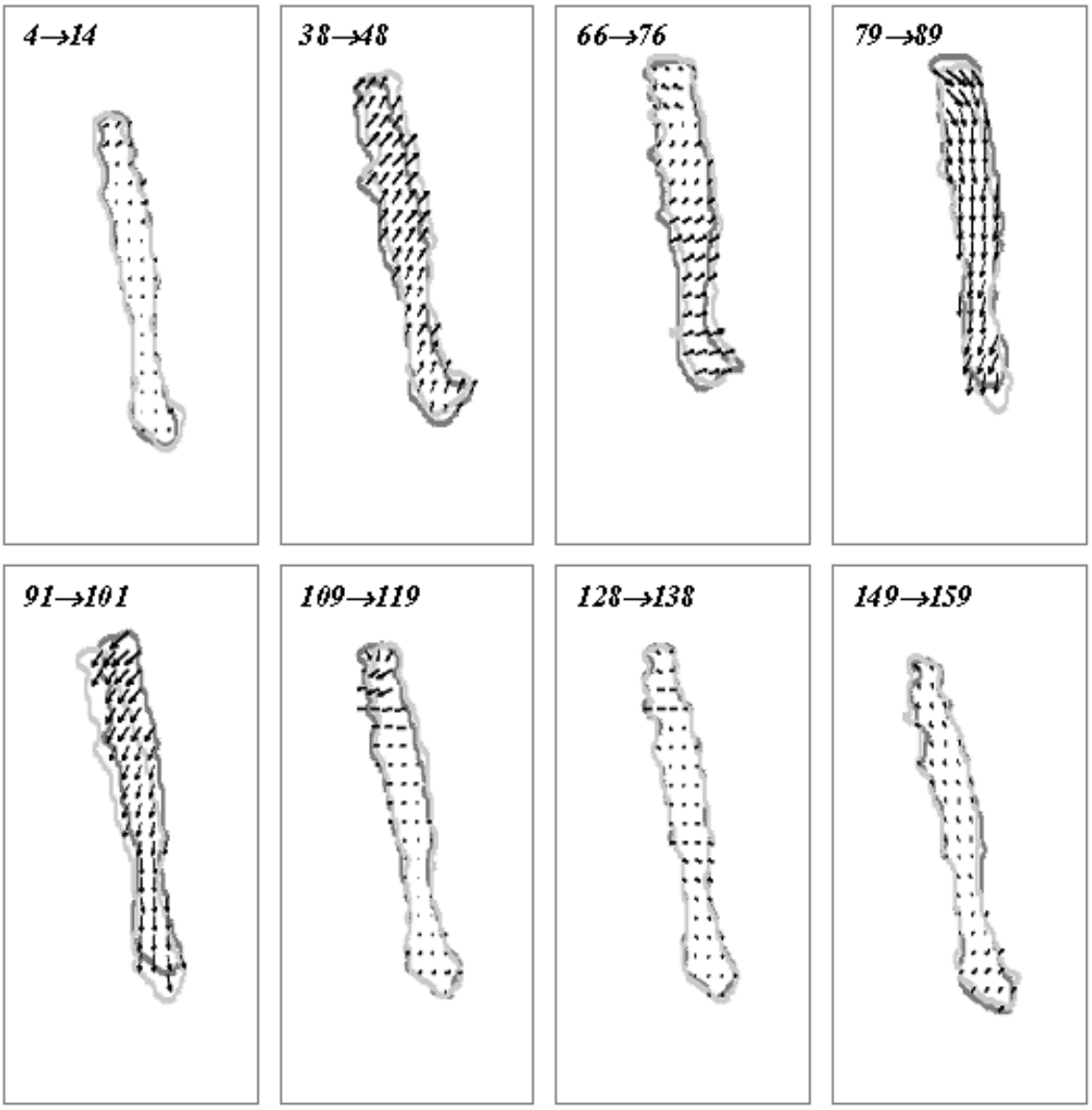

Fig. 5. The velocity field estimated from the segmentation. For better viewing, vectors show the displacement between the current frame f and frame $f + 10$, and the images have not been sector reconstructed. The obtained contours of the muscle in frame f (dark gray) and in frame $f + 10$ (light gray) are also shown.

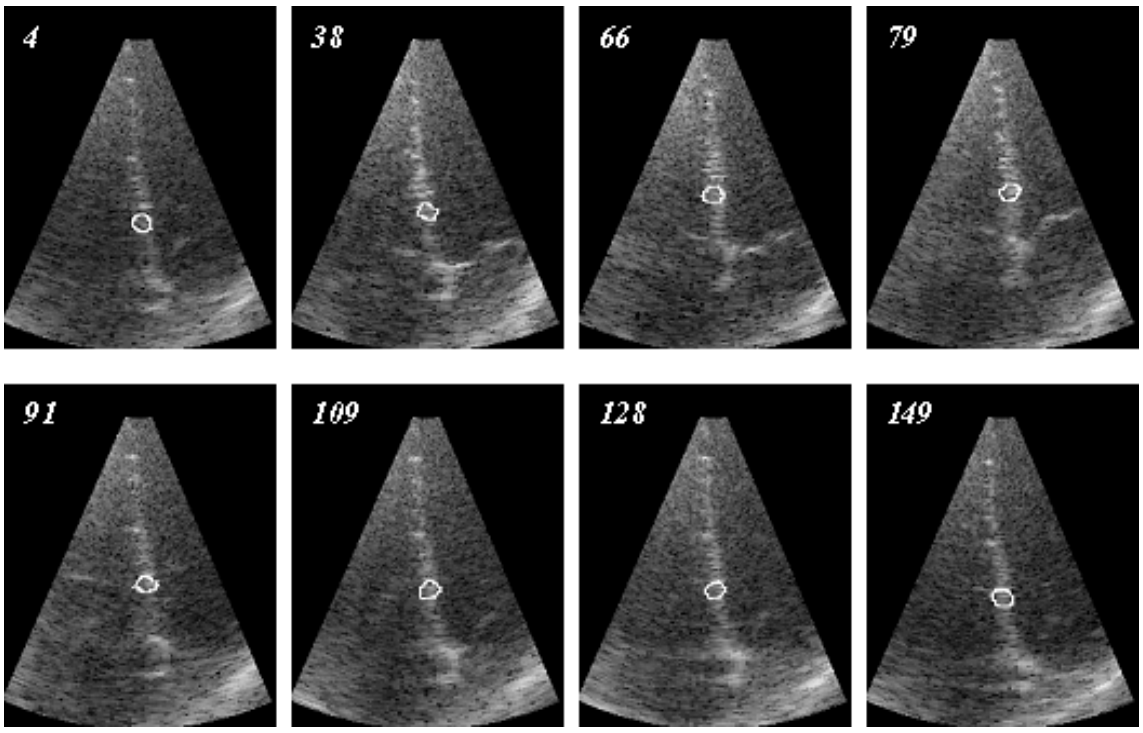

Fig. 6. Tracking of a region of interest throughout the sequence.

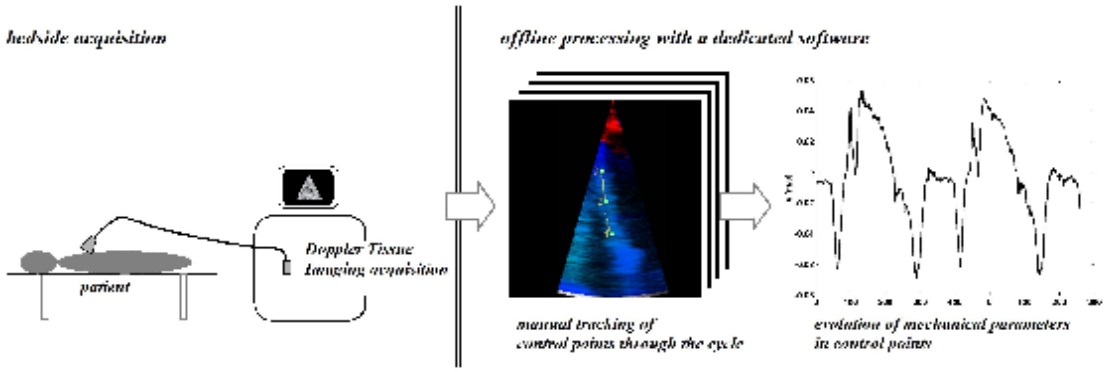

Fig. 7. Scheme summarizing the procedure performed by the cardiologist to derive the temporal evolution of mechanical parameters of the tissue in regions of the myocardium. This procedure requires a stage of manual tracking of control points through the cardiac sequence

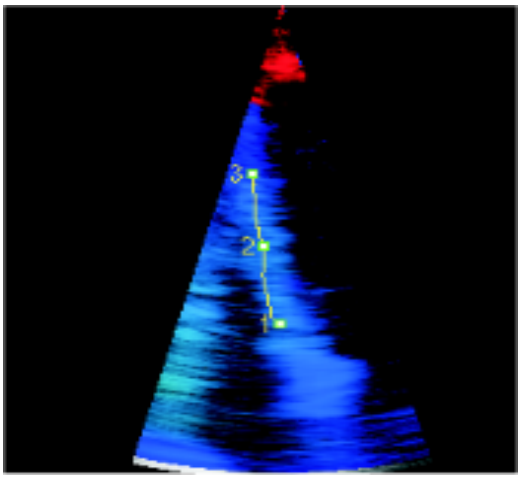

Fig. 8. A screen shot from the software dedicated to tracking control points through the cardiac cycle: the control points have to be moved manually by the cardiologist in consecutive frames of the sequence.

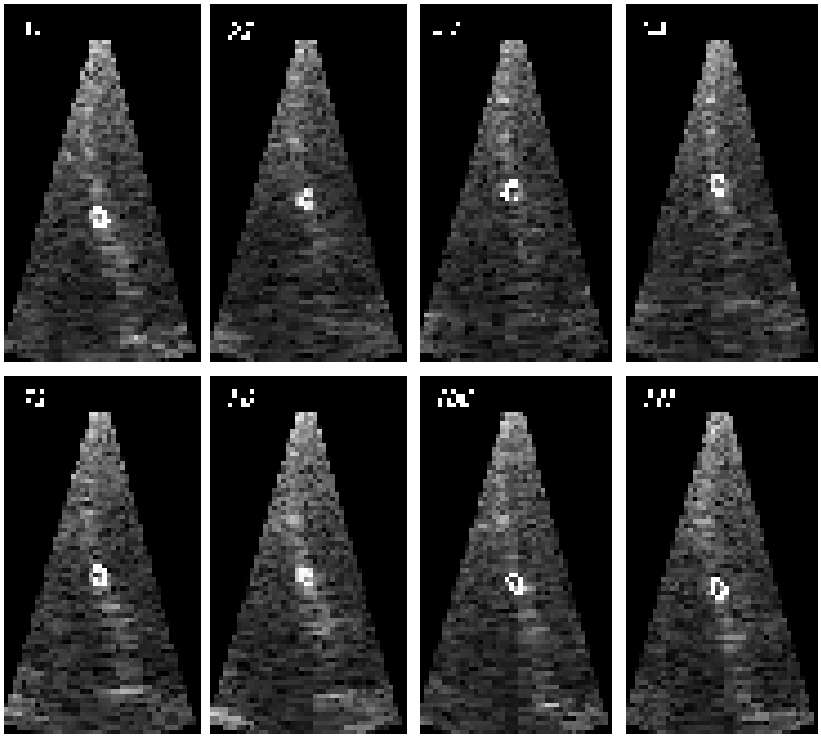

Fig. 9. Tracking of a region of interest, in eight frames extracted from the sequence, covering one cardiac cycle.

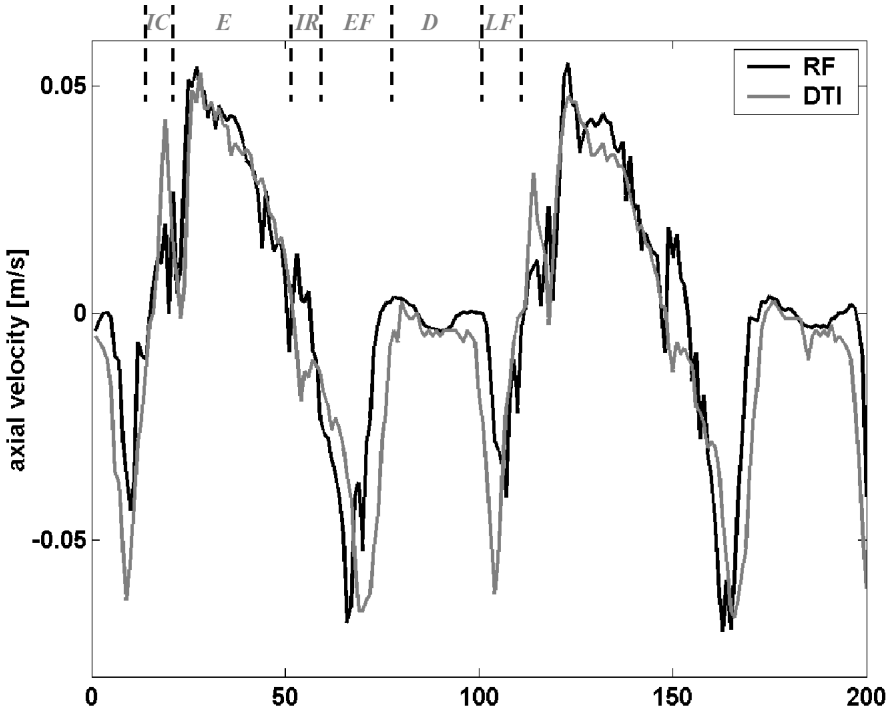

Fig. 10. Evolution of the axial velocity in the positions of the region of interest obtained with the proposed method (black) and the reference curve provided by the expert cardiologist (gray; due to the different sampling rate of the two data, this last curve has been down-sampled to 98 fps). On top of the figure, positions of cardiac events are approximately indicated: isovolumetric contraction (IC), ejection (E), isovolumetric relaxation (IR), early filling (EF), diastasis (D) and late filling (LF).